2012

Gold-platinum alloys and Vegard's law on the nanoscale

PHYSICAL REVIEW B, COLLEGE PK, v. 86, n. 24, supl. 1, Part 6, pp. 2877-2884, DEC 17, 2012
http://www.producao.usp.br/handle/BDPI/35922

PHYSICAL REVIEW B **86**, 241403(R) (2012)

Gold-platinum alloys and Vegard's law on the nanoscale

L. Leppert,[1] R. Q. Albuquerque,[1,2] and S. Kümmel[1,*]
[1]*Theoretical Physics IV, University of Bayreuth, D 95440 Bayreuth, Germany*
[2]*Institute of Chemistry of São Carlos, University of São Paulo, 13560-970 São Carlos-SP, Brazil*
(Received 10 August 2012; published 17 December 2012)

The structure of gold-platinum nanoparticles is heavily debated as theoretical calculations predict core-shell particles, whereas x-ray diffraction experiments frequently detect randomly mixed alloys. By calculating the structure of gold-platinum nanoparticles with diameters of up to ≈3.5 nm and simulating their x-ray diffraction patterns, we show that these seemingly opposing findings need not be in contradiction: Shells of gold are hardly visible in usual x-ray scattering, and the interpretation of Vegard's law is ambiguous on the nanoscale.

DOI: 10.1103/PhysRevB.86.241403 PACS number(s): 36.40.−c, 61.46.Hk, 61.05.cf

Nanoparticles (NPs) made of noble metals have proven to be excellent catalysts.[1–8] Alloy particles from gold (Au) and platinum (Pt) are of particular interest, as they show enhanced catalytic behavior in important oxidation reactions.[9–17] They allow these reactions to take place under mild conditions, thus offering hope for materials' synthesis with minimal ecological impact. These enticing prospects, however, are clouded by a lack of understanding of Au-Pt nanoalloys that extends even to such an elementary property as their structure. There appears to be a serious discrepancy between theory and experiment: Theoretical calculations find core-shell particles as the energetically lowest pattern,[18–23] whereas x-ray diffraction typically detects randomly mixed alloys.[13,24–27] By calculating the structure and x-ray diffraction patterns of Au-Pt NPs we show here that shells of Au are poorly visible in the x-ray patterns and that Vegard's law is ambiguous on the nanoscale.

Vegard's law states that the lattice constant in a bulk binary alloy results from linear interpolation between the lattice constants of the pure constituent elements.[28] The interpolation factor is given by the ratio of the constituents' concentrations, e.g., in a half-and-half alloy the alloy's lattice constant is just the average of the lattice constants of the two pure metals. The analysis of x-ray scattering peaks from which it is concluded that experimentally generated Au-Pt particles are not core-shell structures relies on Vegard's law: One expects to observe two peaks in bimetallic core-shell or segregated particles and concludes that the particle is a random alloy if only one clear peak is observed (for each set of Miller indices and assuming indexing as in a bulk lattice). From the scattering angle one deduces the lattice constant. The latter is then translated into an Au/Pt ratio with the help of Vegard's law. Inherent to this procedure is the assumption that Vegard's law is valid only for random alloys.

In this article we check the validity of this procedure via theoretical simulation. The intensity I of the radiation scattered by an ensemble of atoms is given by Debye's scattering equation,[29]

$$I = \sum_m \sum_n f_m f_n \frac{\sin k r_{mn}}{k r_{mn}}, \tag{1}$$

where f are the atomic form factors of atoms labeled with m and n (form factors for Au and Pt taken from Ref. 30), $r_{mn} = |\mathbf{r}_m - \mathbf{r}_n|$ is the distance between two atoms at positions $\mathbf{r}_m$ and $\mathbf{r}_n$, and $k = 4\pi \sin\theta/\lambda$ is the wave number. In the latter, θ denotes the scattering angle and λ the wavelength (here, 1.5 Å). The challenge for the theoretical analysis lies in the need to investigate particles of the relevant[13,25,26] size of up to 3–4 nm, i.e., several hundred Au and Pt atoms, while also being able to cover different structures and sizes to be able to identify universal effects and trends.

For coping with these challenges we employ density functional theory (DFT) and molecular dynamics (MD). DFT allows us to obtain the electronic structure from first principles. We use the Perdew-Burke-Ernzerhof generalized gradient approximation[31] and take relativistic effects into account via a scalar-relativistic effective core potential.[32–34] However, for structure optimizations computational effort limits DFT to Au-Pt clusters with several tens of atoms (≈1000 valence electrons). MD allows for geometry optimizations also for much larger systems. In our MD the potential energy is described by the many-body Sutton-Chen potential.[35] From the Sutton-Chen parameters for the Au-Au and Pt-Pt interactions the parameters for the Au-Pt interactions were obtained by a combination rule.[36] Further details can be found in the Supplemental Material[37] and references therein.[38–42] As Eq. (1) translates interatomic distances into the peaks of the simulated x-ray patterns, it is a decisive question whether the trends of the differences between Au-Au, Au-Pt, and Pt-Pt bond lengths that are obtained from the MD potentials are reliable. As a test we have compared MD and DFT for 20-atomic tetrahedral and amourphous structures,[21] several 38-atomic clusters, and the 60-atomic particle $Au_{22}Pt_{38}$ (see structures depicted in Fig. 4). The comparisons (see the Supplemental Material[37] for details) reveal that MD bond lengths are consistently smaller than DFT ones for small clusters. This is plausible, as the MD potential parameters were obtained by fitting to much larger (bulk) systems. The important and reassuring finding, though, is that the trends with respect to bond length differences are quite similar. For both methods the general finding is that Au-Au bonds are longest and Pt-Pt bonds are shortest, with Au-Pt falling in between. Also, the differences among the average lengths of Au-Au bonds, Au-Pt bonds, and Pt-Pt bonds that one finds in randomly mixed and core-shell particles are small in both methods. As the quantitative accuracy of MD-based bond length prediction is expected to improve further for larger systems due to the way in which the MD parameters were optimized, we expect the MD bond length distribution to be reasonably reliable for the large NPs which we address in the following.

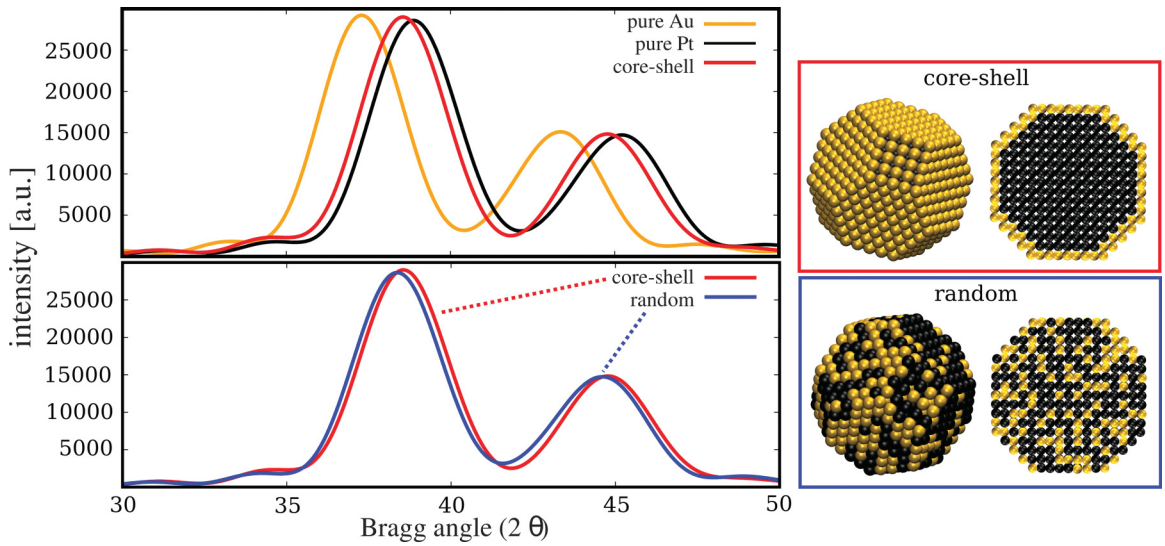

FIG. 1. (Color online) Left: Calculated x-ray scattering patterns of pure Au, Pt, and core-shell NP (top) and core-shell and randomly mixed NP (bottom). Right: View of the core-shell (top) and randomly mixed (bottom) NP (outside and cross section).

We thus turn to the experimentally relevant nanoalloys. We first focus on truncated octahedral structures, because it is known that frequently experimental structures are faceted and bulk-like.[13,25,26] Changes in the NPs' structures are considered when we take into account finite temperatures. With 1289 atoms we constructed octahedra with a diameter of about 3.5 nm and of randomly mixed and of Pt-core Au-shell type. For both types we used the composition $Au_{484}Pt_{805}$, because it allows for a complete shell of Au and a sizable percentage of both atomic species in the NPs. Both types of starting structures were first relaxed at 1 K and then propagated for 500 ps at a temperature of 300 K in MD runs in a canonical ensemble using an Evans' thermostat[43] and vacuum boundary conditions. Every 20 ps a structure "snapshot" was taken. These structures were then optimized with a conjugate gradient procedure. The core-shell structure is 36.57 eV lower in total energy than the lowest randomly mixed configuration. For each type of structure the optimized geometry with the lowest energy was taken as the final structure for the further analysis.

Analyzing the average bond lengths shows that in the core-shell cluster the large Pt core dominates the bond length distribution, with an average Pt-Pt distance of 2.77 Å. The mean Au-Au distance in the single Au shell is the same as the mean Pt-Pt bond length. This finding is reminiscent of the lattice deformation and matching that one encounters when growing single layers of one material on a substrate with a different lattice constant. The Au-Pt distance of 2.78 Å is slightly larger, allowing the shell to wrap around the core. The bond length most often encountered in the randomly mixed NP is one that falls in between the Au-Au and the Pt-Pt bond length, with Au-Pt bonds on average being 2.76 Å, Au-Au bonds 2.79 Å, and Pt-Pt bonds 2.74 Å.

Based on these structures we take the decisive step and compute the x-ray diffraction pattern according to Eq. (1). The top left panel in Fig. 1 shows the pattern that one obtains from pure Au or pure Pt NPs with 1289 atoms in orange and black, respectively. Figure 1 shows the first two main peaks, corresponding to the experimentally observed regime. The red line shows the x-ray pattern for the core-shell NP. As elaborated previously the expectation so far has been to find separate peaks for this type of structure, as it has separate Au and Pt phases. Yet, no double-peak structure is observed at all; the peak shapes for the different NPs are nearly identical. Our first important conclusion therefore is that a core-shell structure in NPs does not necessarily lead to separate x-ray peaks for the different phases. The lower left panel shows the second important result: The x-ray pattern for the core-shell NP (as above) and the one for the randomly mixed NP are very similar. Core-shell structures may thus be hard to detect via x-ray scattering.

However, we now take the analysis one step further and go through the Vegard's-law-based analysis of the x-ray data. Assuming that Miller indices (hkl) can be assigned as in the bulk—an assumption which is reasonably well justified for the faceted NPs studied here and in experiments—one can use the Bragg scattering equation $a = \lambda(h^2 + k^2 + l^2)/(2 \sin\theta)$ to determine the lattice constant a from the scattering angle. For pure NPs the x-ray analysis leads to a lattice constant of 4.06 Å for Au and 3.90 Å for pure Pt. These are very close to the pure bulk values, i.e., the Vegard's-law-based analysis correctly identifies the NPs as pure ones. This result also confirms our procedure for building the particles and calculating the x-ray patterns. The decisive question now is how well the procedure works when we translate the x-ray pattern obtained for the bimetallic NPs into lattice constants and the relative Au and Pt content using Vegard's law as explained above. If this type of interpretation is accurate, then it should yield exactly 38% of Au and 62% of Pt, corresponding to the $Au_{484}Pt_{805}$ particles that we constructed. Yet, for the core-shell particle the a deduced from the x-ray pattern is 3.94 Å, and the Vegard's-law-based analysis translates this into an Au content of ca. 19 %. Thus, it underestimates the Au content by a factor of 2. This is a serious misprediction. For the randomly mixed particle the situation is better, yet not perfect, with an a of 3.95 Å being translated into an Au content of 31 %. In order to further elucidate the situation we constructed an 1289-atom

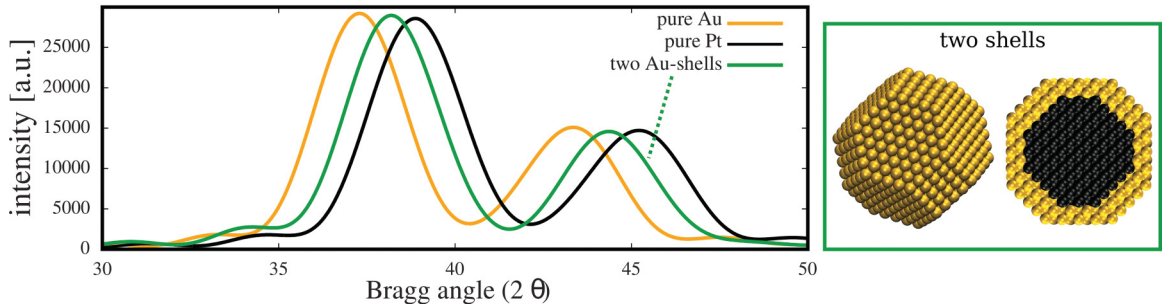

FIG. 2. (Color online) Calculated x-ray scattering patterns (left) and visualization (right) of a core-shell NP with two shells of Au.

NP with two layers of Au, following the same MD procedure as described above. The resulting particle $Au_{830}Pt_{459}$ has an Au content of 64 %. A Vegard's-law-based analysis of the x-ray pattern (see Fig. 2) is again far off the mark. It predicts an a of 3.97 Å, corresponding to 44 % of Au. Thus, instead of showing that the particle contains more Au than Pt, the x-ray analysis leads one to believe that the NP contains more Pt than Au.

In judging the significance of these results one should recall that our analysis so far has been conducted under ideal conditions, as our calculated x-ray patterns stem from monodisperse, zero-temperature particles. In actual experiments the uncertainties in determining the NPs' Au and Pt content from Vegard's law can be larger than the discrepancies that we find here. One can thus imagine that an Au-Pt core-shell particle with roughly one shell of Au might be classified as almost-pure Pt. It may thus appear less puzzling that Pt-core/Au-shell NPs have rarely been found in experimental x-ray analysis despite their theoretical prediction.

In order to estimate the effects that temperature may have and to explicitly check what influence the presence of different structures has on the x-ray pattern, we performed constant-temperature MD simulations as described above, in each case starting from the lowest energy configuration and thermalizing the particle for 1 ns at 1, 50, 100, 200, 250, 300, 600, and 1400 K, respectively. From the last 400 000 steps of each simulation we took 10 structures, each one being 40 000 time steps of 1 fs distant from the previous one. For each of the structures we calculated the x-ray pattern and then superimposed the patterns of a given temperature. Figure 3 shows these finite-temperature diffraction patterns. The first, expected observation is that the peak heights are reduced. At 1400 K the pattern is also considerably broadened, corresponding to a much wider bond length distribution compared to that at lower temperatures. As the melting point of the core-shell particle lies at ca. 1200 K, we observe randomly mixed structures at 1400 K, whereas for the lower temperatures the core-shell mixing pattern is retained, though with an increasingly softening surface.

A further observation to be made in Fig. 3 is that the peaks for elevated temperatures are shifted, and while some shift is expected due to thermal expansion, the magnitude of the shift is much larger than one would expect based on the bulk expansion coefficient. Therefore, we calculated the linear thermal expansion coefficient by evaluating the temperature dependence of the mean interatomic distance.[44] The average thermal expansion coefficient that we obtain in this way up to 600 K is ca. 19×10^{-6} K^{-1}, i.e., considerably larger than that of bulk Au (ca. 14×10^{-6} K^{-1}) and bulk Pt (ca. 9×10^{-6} K^{-1}). We also see that the surface atoms contribute the most strongly to the expansion. Thus, NPs at finite temperatures are likely to have a "diffuse" surface, and this may contribute to their special catalytic properties.

Finally, having demonstrated the limits of traditional x-ray analysis for Au-Pt NPs, we exploit the strength of theoretical simulations to offer direct access to bond length distributions. Thus, we can take a yet closer look at Vegard's law. Figure 4 shows the average bond length as obtained from DFT-based

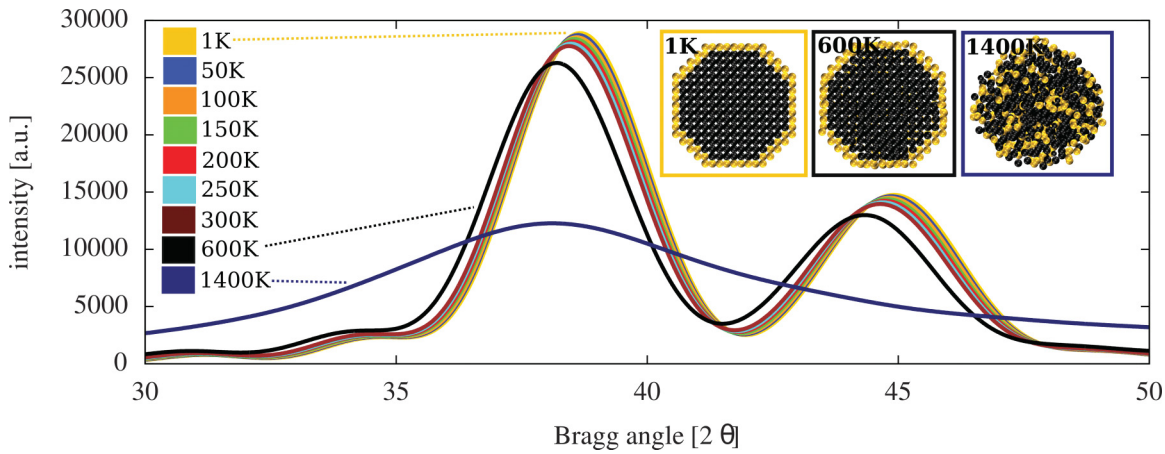

FIG. 3. (Color online) Average NP x-ray scattering patterns at temperatures of 1, 50, 100, 150, 200, 250, 300, 600, and 1400 K. Inset: NP cross sections at 1, 600, and 1400 K.

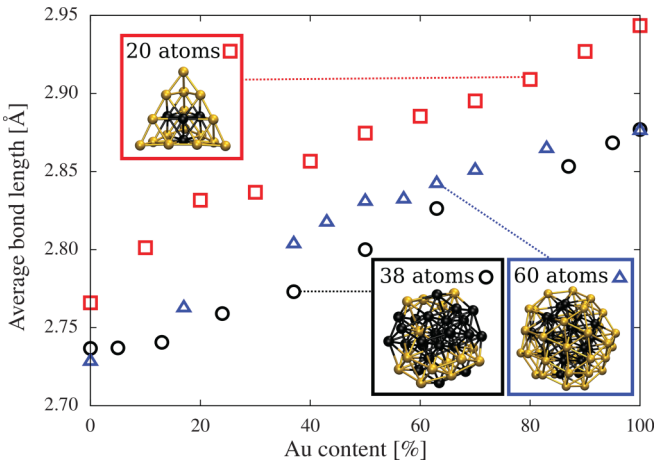

FIG. 4. (Color online) Average nearest-neighbor bond length of 20-, 38-, and 60-atom core-shell-like clusters with varying Au contents.

geometry optimizations for 20-, 38-, and 60-atom particles as a function of the Au content. For the 20-atom clusters we used tetrahedral core-shell geometries,[21] the randomly mixed 38-atom clusters are truncated octahedra,[37] and the 60-atom core-shell clusters are based on an $Au_{30}Pt_{30}$ NP taken from Ref.[22], in which we successively replaced Au withy Pt, and vice versa, followed by a reoptimization of every structure. The striking observation in Fig. 4 is that for all particles, independent of the size and of whether the atoms are core shell or randomly distributed, the average bond length increases linearly with increasing Au content. Thus, one might say that for small particles Vegard's law is valid not only for randomly distributed alloys, but also for other types of bimetallic Au-Pt particles, independently of the specific way in which the atoms are arranged.

In conclusion, we have shown that Vegard's law is ambiguous on the nanoscale, as it may hold not only for random alloys. However, more importantly, we have shown that Vegard's law does not translate into x-ray peaks in the way that has so far been assumed. Even under the ideal conditions that can theoretically be realized an Au-shell in core-shell NPs is poorly visible in x-ray scattering. The Au content of core-shell particles is greatly underestimated when analyzing x-ray diffraction patterns based on Vegard's law. Finite-temperature simulations showed that thermal expansion in 3.5-nm Au-Pt NPs is much greater than in the bulk and affects surface atoms the most strongly. Our findings relativize doubts about theoretical structure predictions that were triggered by the missing experimental verification. The fact that the low-energy structures theoretically predicted for free Au-Pt NPs undoubtedly are core-shell structures still does not exclude the possibility that true Au-Pt nanoalloys form in experiments.[45] The theoretical findings suggest that the existence of Au-Pt nanoalloys, and possibly also of other binary systems,[46,47] in experiments may be linked to effects beyond the ones present in free particles. These may be external influences such as solvents, supports, and special preparation procedures, possibly in combination with entropical contributions which, at finite temperatures, can limit the probability of observing the lowest energy configuration.

We are grateful to R. L. Johnston for providing us with coordinates, to M. Ballauff and J. Breu for discussions, and to DFG SFB 840 for financial support.

*stephan.kuemmel@uni-bayreuth.de

[1] M. Haruta, Catal. Today **36**, 153 (1997).
[2] A. Sanchez, S. Abbet, U. Heiz, W.-D. Schneider, H. Häkkinen, R. N. Barnett, and U. Landman, J. Phys. Chem. A **103**, 9573 (1999).
[3] P. Pyykkö, Ang. Chem. (Int. Ed.) **43**, 4412 (2004).
[4] A. S. K. Hashmi, Chem. Rev. **107**, 3180 (2007).
[5] A. A. Herzing, C. J. Kiely, A. F. Carley, P. Landon, and G. J. Hutchings, Science **321**, 1331 (2008).
[6] M. Schrinner, M. Ballauff, Y. Talmon, Y. Kauffmann, J. Thun, M. Möller, and J. Breu, Science **323**, 617 (2009).
[7] Y. Gao, N. Shao, Y. Pei, and X. C. Zeng, Nano Lett. **10**, 1055 (2010).
[8] E. C. Beret, L. M. Ghiringhelli, and M. Scheffler, Faraday Discuss. **152**, 153 (2011).
[9] Y. Lou, M. M. Maye, L. Han, J. Luo, and C.-J. Zhong, Chem. Commun. **2001**, 473 (2001).
[10] D. Mott, J. Luo, P. Njoki, Y. Lin, L. Wang, and C. Zhong, Catal. Today **122**, 378 (2007).
[11] P. Hernandez-Fernandez, S. Rojas, P. Ocon, J. Gomez de la Fuente, J. San Fabian, J. Sanza, M. Pena, F. Garcia-Garcia, P. Terreros, and J. Fierro, J. Phys. Chem. C **111**, 2913 (2007).
[12] J. Zhang, H. Ma, D. Zhang, P. Liu, F. Tian, and Y. Ding, Phys. Chem. Chem. Phys. **10**, 3250 (2008).
[13] M. Schrinner, S. Proch, Y. Mei, R. Kempe, N. Miyajima, and M. Ballauff, Adv. Mater. **20**, 1928 (2008).
[14] G. Selvarani, S. V. Selvaganesh, S. Krishnamurthy, G. V. M. Kiruthika, P. Sridhar, S. Pitchumani, and A. K. Shukla, J. Phys. Chem. C **113**, 7461 (2009).
[15] Z. Peng and H. Yang, Nano Res. **2**, 406 (2009).
[16] D. F. Yancey, E. V. Carino, and R. M. Crooks, J. Am. Chem. Soc. **132**, 10988 (2010).
[17] B. Du, O. Zaluzhna, and Y. J. Tong, Phys. Chem. Chem. Phys. **13**, 11568 (2011).
[18] H. B. Liu, U. Pal, and J. A. Ascencio, J. Phys. Chem. C **112**, 19173 (2008).
[19] N. Braidy, G. R. Purdy, and G. A. Botton, Acta Mater. **56**, 5972 (2008).
[20] B. H. Morrow and A. Striolo, Phys. Rev. B **81**, 155437 (2010).
[21] L. Leppert and S. Kümmel, J. Phys. Chem. C **115**, 6694 (2011).
[22] A. Logsdail, L. O. Paz-Borbón, and R. L. Johnston, J. Comp. Theo. Nano. **6**, 857 (2009).
[23] D. T. Tran and R. L. Johnston, Proc. R. Soc. A **467**, 2004 (2011).
[24] G. De and C. N. R. Rao, J. Mater. Chem. **15**, 891 (2005).
[25] J. Luo, M. M. Maye, V. Petkov, N. N. Kariuki, L. Wang, P. Njoki, D. Mott, Y. Lin, and C.-J. Zhong, Chem. Mater. **17**, 3086 (2005).
[26] J. Luo, P. N. Njoki, Y. Lin, D. Mott, L. Wang, and C.-J. Zhong, Langmuir **22**, 2892 (2006).
[27] O. Malis, M. Radu, D. Mott, B. Wanjala, J. Luo, and C.-J. Zhong, Nanotechnology **20**, 245708 (2009).

[28]L. Vegard, Z. Phys. **5**, 17 (1921).
[29]P. Debye, Ann. Phys. **348**, 49 (1913).
[30]A. J. C. Wilson and E. Prince (eds.), *International Tables for Crystallography* Vol. III, 2nd. ed. (Kluwer Academic, Boston, 1999), p. 556.
[31] J. P. Perdew, K. Burke, and M. Ernzerhof, Phys. Rev. Lett. **77**, 3865 (1996).
[32]D. Andrae, M. Dolg, H. Stoll, and H. Preub, Theor. Chim. Acta **77**, 123 (1990).
[33]R. Ahlrichs, M. Bär, M. Häser, H. Horn, and C. Kölmel, Chem. Phys. Lett. **162**, 165 (1989).
[34]TURBOMOLE V5.10 (2008).
[35]A. P. Sutton and J. Chen, Philos. Mag. Lett. **61**, 139 (1990).
[36]Z. Yang, X. Yang, and Z. Xu, J. Phys. C **112**, 4937 (2008).
[37]L. Leppert, R. Albuquerque, and S. Kümmel, See Supplemental Material at http://link.aps.org/supplemental/10.1103/PhysRevB.86.241403 for computational details.
[38]S. J. Mejia-Rosales, C. Fernandez-Navarro, E. Perez-Tijerina, J. M. Montejano-Carrizales, and M. Jose-Yacaman, J. Phys. Chem. B **110**, 12884 (2006).
[39]S. K. R. S. Sankaranarayanan, V. R. Bhethanabotla, and B. Joseph, Phys. Rev. B **71**, 195415 (2005).
[40]Z. Yang, X. Yang, Z. Xu, and S. Liu, Phys. Chem. Chem. Phys. **11**, 6249 (2009).
[41]P. H. Hünenberger, Adv. Polym. Sci. **173**, 105 (2005).
[42]F. Furche, R. Ahlrichs, P. Weis, C. Jacob, S. Gilb, T. Bierweiler, and M. M. Kappes, J. Chem. Phys. **117**, 6982 (2002).
[43]D. J. Evans and G. P. Morriss, Comp. Phys. Rep. **1**, 297 (1984).
[44]S. Kümmel, J. Akola, and M. Manninen, Phys. Rev. Lett. **84**, 3827 (2000).
[45]V. Petkov, B. N. Wanjala, R. Loukrapam, J. Luo, L. Yang, C. Zhong, and S. Shastria, Nano Lett. **12**, 4289 (2012).
[46]J. Kaiser, L. Leppert, H. Welz, F. Polzer, S. Wunder, N. Wanderka, M. Albrecht, T. Lunkenbein, J. Breu, S. Kümmel, Y. Lu, and M. Ballauff, Phys. Chem. Chem. Phys. **14**, 6487 (2012).
[47]J. Hermannsdörfer, M. Friedrich, N. Miyajima, R. Q. Albuquerque, S. Kümmel, and R. Kempe, Angew. Chem. (Int. Ed.) **51**, 11473 (2012).